catalysts

MDPI

Article

Core/Shell Nitrogen-Doped TiO_2@SiO_2 Nano-Catalyst as an Additive in Photocatalytic Paint for Gaseous Acetaldehyde Decomposition

Suwapee Samangsri [1,2], Thanita Areerob [3] and Siriluk Chiarakorn [4,5,*]

1 The Joint Graduate School of Energy and Environment, King Mongkut's University of Technology Thonburi, Bangkok 10140, Thailand
2 Center of Excellence on Energy Technology and Environment, PERDO, Bangkok 10140, Thailand
3 Marine Environmental and Geoinformatics Technology Research Unit, Faculty of Technology and Environment, Prince of Songkla University Phuket Campus, Phuket 83120, Thailand
4 Environmental Technology Program, School of Energy, Environment and Materials, King Mongkut's University of Technology Thonburi, Bangkok 10140, Thailand
5 Environmental and Energy Management for Community and Circular Economy (EEC&C) Research Group, King Mongkut's University of Technology Thonburi, Bangkok 10140, Thailand
* Correspondence: siriluk.chi@kmutt.ac.th; Tel.: +66-2470-8654

Abstract: A nitrogen-doped TiO_2@SiO_2 core/shell nano-photocatalyst (N-TiO_2@SiO_2) was used as an additive in photocatalytic paint and applied for the photocatalytic degradation of gaseous acetaldehyde under light-emitting diode (LED) visible light irradiation. N-TiO_2 was synthesised via the solvothermal method and then encapsulated by SiO_2 via the sol-gel method. The incorporation of the N atom into the TiO_2 structure was observed by X-ray photoelectron spectroscopy. The N-TiO_2@SiO_2 core/shell structure was determined by TEM images. The photodegradation of gaseous acetaldehyde using the prepared N-TiO_2@SiO_2 photocatalytic paint was examined in a closed chamber under LED light irradiation. The photodegradation of acetaldehyde by N-TiO_2@SiO_2 photocatalytic paint (31%) was significantly higher than that of TiO_2 paint (5%) and N-TiO_2 paint (20%) within 16 h. The chemical resistance and adhesion ability of N-TiO_2@SiO_2 photocatalytic paint were investigated following Thai Industrial Standards (TIS) no. 2321 and standard test methods for rating adhesion by tape test (ASTM D 3359-22). The N-TiO_2@SiO_2 paint showed good acid and alkali resistance, as well as high adhesion ability comparable with commercial paint (without a photocatalyst).

Keywords: N-doped titanium dioxide; silica; photocatalytic paint; core/shell photocatalyst; acetaldehyde

Citation: Samangsri, S.; Areerob, T.; Chiarakorn, S. Core/Shell Nitrogen-Doped TiO_2@SiO_2 Nano-Catalyst as an Additive in Photocatalytic Paint for Gaseous Acetaldehyde Decomposition. *Catalysts* **2023**, *13*, 351. https://doi.org/10.3390/catal13020351

Academic Editors: Xiangjiu Guan and Shichao Zong

Received: 30 December 2022
Revised: 30 January 2023
Accepted: 2 February 2023
Published: 4 February 2023

1. Introduction

Today, indoor air quality (IAQ) has become a significant public concern. Most people spend 80–90% of their time living indoors such as in households, vehicles, shopping centres, and offices [1–4]. The significant parameters that affect IAQ include the construction materials and furniture in households, as well as the human activities in buildings [5,6]. Indoor air pollution (IAP) includes NO_x, volatile and semi-volatile organic compounds (VOCs), SO_2, O_3, CO, PM, radon, toxic metals, and microorganisms. The sources of VOCs are mostly generated from human activities indoors, such as cooking, solvent use, cleaning reagent use, tobacco smoke, etc. [7,8]. Due to their low boiling point, they are easily volatile at room temperature and accumulate in indoor environments. Short-term exposure to VOCs can cause adverse effects on human health, including headache and nausea as well as eye, nose, and throat irritation. These symptoms are commonly attributed to sick-building syndrome (SBS) [9]. Chronic exposure to VOCs can lead to serious health problems, such as failure of the liver and kidneys, respiratory diseases, and cancer [10]. The common VOCs found in indoor air include benzene, toluene, formaldehyde, acetaldehyde, etc. Acetaldehyde is a major compound in tobacco smoke [11–13]. The United States Environmental Protection

Agency discovered that tobacco smoke accumulated more indoors than it did outside [14], indicating that people are subjected to a higher risk of exposure to acetaldehyde indoors than they would be outside. Thus, acetaldehyde is one of the most significant VOCs in households and office buildings.

Various VOCs treatments have been studied, such as filtration [15], adsorption [16], ozonation [17], and photocatalysis [18]. Among these treatment methods, the photocatalytic reaction is one of the most promising applications for VOC purification. Photocatalysis is the acceleration of a photo-induced reaction by a catalyst. Photocatalytic processes have four steps, including (i) stimulation of the photocatalyst by light adsorption, (ii) generation of the electron (e^-) and hole (h^+) in the valence band (VB) and conduction band (CB), (iii) the electron (e^-) reacts with oxygen (O_2) while the hole (h^+) reacts with water (H_2O) and produces superoxide radicals (O_2^-) and hydroxyl radicals ($OH^\bullet$), respectively, and (vi) both O_2^- and $OH^\bullet$ oxidise and reduce the pollutants [19,20]. Titanium dioxide (TiO_2) is a common photocatalyst widely used for photocatalytic applications [21]. It possesses many advantages compared with other photocatalysts, such as low cost [22], good stability [23], and environmental responsiveness [24]. Many studies have focused on using TiO_2 as an additive in surface coating applications. Islam et al., (2020) [25] developed photocatalytic paint based on TiO_2 nanoparticles and acrylate-based photopolymer resin. They found that the TiO_2 embedded in the polymer could generate $OH^\bullet$ under UV-B light and sunlight, enabling 80–90% photocatalytic degradation of methylene blue (MB) and methyl orange (MO) under sunlight and UV-B light. Basso et al., (2020) [26] produced photocatalytic paint by adding TiO_2 P25 powder to an acrylic-based paint. The photocatalytic paint could reduce toluene with a photocatalytic efficiency of 15% under UV light. At present, TiO_2 is commercially used in photocatalytic paints to provide a self-cleaning function. However, it is known that TiO_2 photocatalytic paint involves drawbacks, including (1) limited photocatalytic performance of TiO_2 under visible light irradiation in an indoor environment and (2) self-degradation when adding bare TiO_2 to acrylic paint due to degradation of the organic binder in the paint.

An alternate approach to enhance the photocatalytic performance of TiO_2 under visible light irradiation is nitrogen doping. Meroni et al., (2011) [27] modified TiO_2 with nitrogen (N-doped TiO_2) by the sol-gel method. They found that the energy band gap of N-doped TiO_2 was narrower than that of pure TiO_2 due to N species being substitutional and interstitial in the TiO_2 anatase structure. The photodegradation of ethanol and acetaldehyde using N-doped TiO_2 under UV and solar irradiation was then examined. The reaction rate of ethanol and acetaldehyde degradation under UV and solar irradiation by N-doped TiO_2 was higher than that of pure TiO_2. He et al., (2013) [28] studied benzene degradation under UV irradiation using N-doped TiO_2 synthesised via the solvothermal method. The results showed that the N-doped TiO_2 achieved the highest photocatalytic degradation and remained unchanged after being recycled 15 times. After doping, the particle sizes of N-doped TiO_2 significantly decreased and the specific surface area of N-doped TiO_2 significantly increased. Sirivallop et al., (2020) [29] synthesised N-doped TiO_2 using the solvothermal method applied for the degradation of MB and ammonia (NH_3) under LED irradiation. The N-doped TiO_2 provided a narrowing energy band gap, and the photodegradation performance of MB and NH_3 under LED irradiation using N-doped TiO_2 was significantly higher than that of pure TiO_2. It was also found that N-doped TiO_2 had a pale yellow colour. Thus, it could be added to paint without changing the colour tone.

Regarding self-degradation in the paint caused by photocatalysts, encapsulating the highly reactive TiO_2 photocatalyst is recommended. The core/shell technique is a new alternative approach to encapsulating TiO_2 inside inert compounds. With this method, the specific surface area is significantly improved because the core/shell structure can enhance particle distribution and prevent particle agglomerations, which are the key factors in the enhancement of photocatalytic activity [30,31]. Silicon dioxide (SiO_2) is mostly used as a shell due to its unique properties, such as thermal and chemical stability, easy reuse, and

enhanced light transmission with minimum reflection [32]. The advantages of SiO_2 used as a shell in TiO_2@SiO_2 nano-catalyst were increasing specific surface area, protecting TiO_2 aggregation, preventing charge recombination, and providing acid sites on the surface, which could enhance the adsorption capacity and photocatalytic performance of the photocatalytic paint [33]. Mahanta et al., (2022) [34] synthesised TiO_2@SiO_2 photocatalysts by the sol-gel method. The photocatalysts had high crystallinity and a large specific surface area. The TiO_2@SiO_2 photocatalyst was then applied to decolourise methylene blue (MB) under sunlight and UV light. The decolourisation efficiency of MB under sunlight and UV light using TiO_2@SiO_2 was approximately 90% and 85%, respectively. Wang et al., (2020) [35] synthesised TiO_2@SiO_2 photocatalyst and coated it on a cement substrate for the decomposition of pollutants in outdoor environments. The photocatalytic performance of TiO_2@SiO_2 coated on cement was evaluated by the decolourisation of rhodamine B (RhB) under UV light irradiation. The results found that the SiO_2 coated on the TiO_2 surface had a large specific surface area. The RhB photodegradation efficiency using TiO_2@SiO_2 coated on cement was approximately 73%, which was higher than that of TiO_2 P25 coated on cement (60%).

This research aims to develop visible-light responsive photocatalytic paint using an N-doped TiO_2-SiO_2 core/shell nano-catalyst (TiO_2@SiO_2) as an additive in emulsion-based paint. N-doped TiO_2 was synthesised by the solvothermal method and then encapsulated with SiO_2 by the sol-gel method. The physical and chemical properties of the photocatalytic paint were tested following Thai Industrial Standards (TIS) and the American Society for Testing and Materials (ASTM). The performance of the photocatalytic paint for the degradation of gaseous acetaldehyde was examined under LED visible light irradiation in a closed chamber.

2. Results and Discussion

2.1. Nano-Photocatalyst Characteristics

2.1.1. Crystalline Structure

The crystalline structures of SiO_2, TiO_2, N-TiO_2, and N-TiO_2@SiO_2 core/shell were determined by the XRD technique (Figure 1). The XRD patterns were identified by Joint Committee on Powder Diffraction Standard. The board XRD peak at 23.5° was observed on the SiO_2 sample, corresponding to standard amorphous silica (JCPDS No. 29-0085), while the diffraction peaks of TiO_2, N-TiO_2, and N-TiO_2@SiO_2 core/shell were similar. The peaks that appeared at 25.3°, 37.8°, and 48.2° were referred to as standard TiO_2 anatase (JCPDS No. 21-1272), at (101), (004), and (200) planes, respectively. No evident peak referring to nitrogen was observed due to low nitrogen content in the N-doped samples, nor could the diffraction peak of SiO_2 be observed. This might have been caused by well-dispersed silica on the surface of the N-TiO_2 photocatalyst.

2.1.2. Surface Morphology

The surface morphology of TiO_2, N-TiO_2, and N-TiO_2@SiO_2 core/shell was examined using TEM images, as shown in Figure 2. The TEM photograph demonstrates the aggregation of TiO_2 (Figure 2a) and N-TiO_2 particles (Figure 2b), while Figure 2c exhibits the core/shell structure of the N-TiO_2@SiO_2 nano-photocatalyst. The SiO_2 shells (thin transparent layers) are uniformly deposited on the N-TiO_2 cores (black spots), resulting in better particle dispersion than that of the N-TiO_2 particles. The SiO_2 shell thickness of the N-TiO_2@SiO_2 core/shell was approximately 20–30 nm. The particle size distribution (see Figure S1 in Supplementary Material) was determined based on the SEM images (see Figure S2 in Supplementary Material). The results showed that the mean particle sizes of TiO_2, N-TiO_2, and N-TiO_2@SiO_2 core/shell were approximately 15–25 nm, 16–22 nm, and 30–40 nm, respectively.

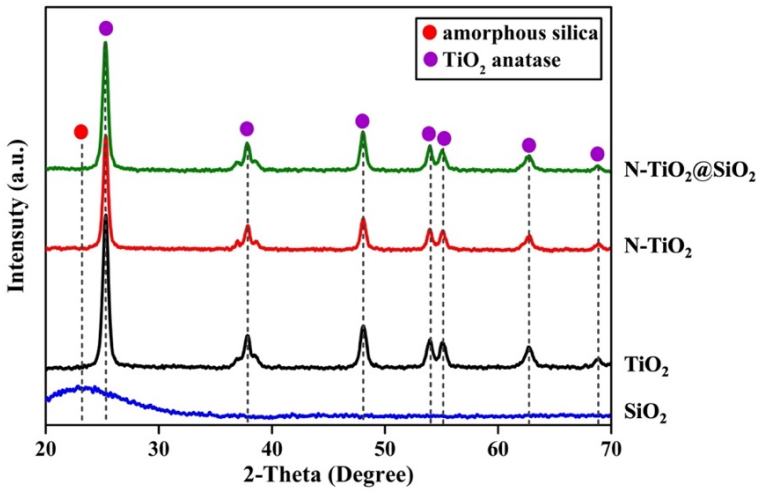

Figure 1. XRD patterns of SiO_2, TiO_2, N-TiO_2, and N-TiO_2@SiO_2.

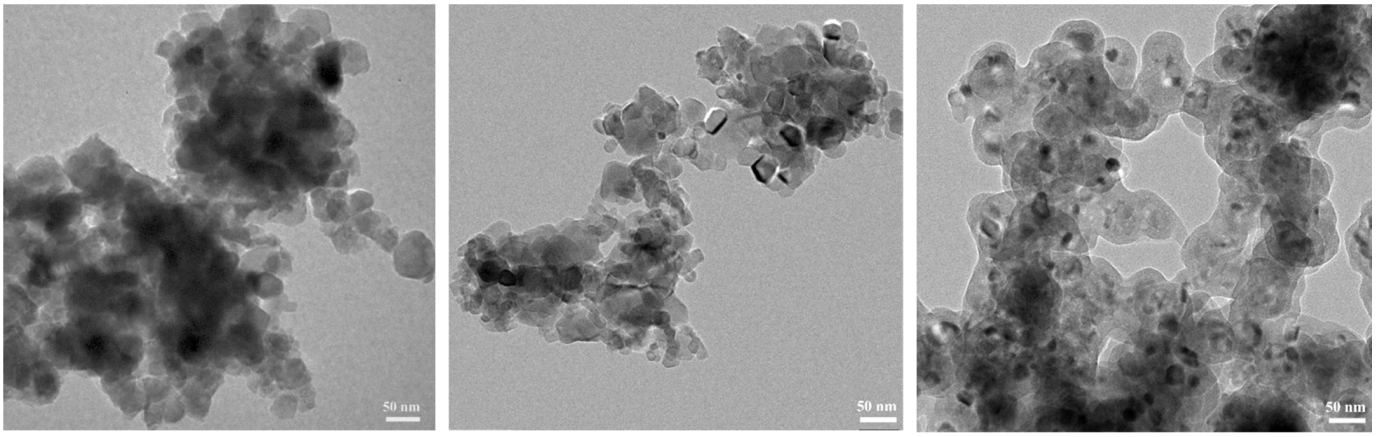

(**a**) (**b**) (**c**)

Figure 2. TEM images of (**a**) TiO_2, (**b**) N-TiO_2, and (**c**) N-TiO_2@SiO_2 core/shell.

2.1.3. Chemical Composition

The EDX spectra were used to indicate the existence of N, Si, and Ti elements in the N-TiO_2@SiO_2 core/shell compared with the N-TiO_2 nano-catalyst, as shown in Figure S3 in Supplementary Material. Furthermore, the XPS analysis (see Figure 3) was used to investigate elemental composition as well as the chemical and electronic states of the elements in the nano-catalysts.

The XPS spectra of TiO_2, N-TiO_2, and N-TiO_2@SiO_2 core/shell, presented in Figure 3a, indicated the Ti 2p peak binding energies for Ti $2p_{1/2}$ and Ti $2p_{3/2}$ [36]. The peaks of Ti $2p_{1/2}$ and Ti $2p_{3/2}$ of TiO_2 were 465 and 459 eV, respectively. It was observed that the Ti $2p_{1/2}$ peak of N-TiO_2 was shifted to a lower binding energy than that of TiO_2. Similarly, the Ti $2p_{1/2}$ peak of N-TiO_2@SiO_2 core/shell was slightly shifted to a lower binding energy than that of N-TiO_2. The shifts in Ti $2p_{1/2}$ spectra were due to the incorporation of N and Si atoms into the TiO_2 structure. The O 1S spectra of all samples, shown in Figure 3b, indicated the Ti-O-Ti bonding (530 eV) in TiO_2, N-TiO_2, and N-TiO_2@SiO_2 core/shell. In addition, the binding energy of the O 1s peak that indicated the interaction between the SiO_2 shell and N-TiO_2 core of the N-TiO_2@SiO_2 nano-catalyst was observed at 532 eV (Ti–O–Si)s, corresponding with the blue shift of the binding energy of the Ti $2p_{3/2}$ peak for N-TiO_2@SiO_2 core/shell [37,38]. The N 1s spectra of N-TiO_2 and N-TiO_2@SiO_2 core/shell also recognised three peaks, corresponding to N–O (403 eV), Ti–O–N (400 eV), and Ti–N–Ti (398 eV) bonding, respectively (Figure 3c). The N–O bonding related to the signal

of nitrogen species [39], while the Ti–O–N and Ti–N–Ti were attributed to the nitrogen interstitial and substitutional incorporation into the TiO_2 lattice, respectively [40,41]. The Si 2p spectrum of N-TiO_2@SiO_2 core/shell displayed in Figure 3d indicated a peak at about 103.36 eV, which was attributed to Si–O–Si [42]. The TEM images and XPS results confirmed the existence of the SiO_2 shell coated on the N-TiO_2 core and indicated the interaction between N, Si, and TiO_2 in the N-TiO_2@SiO_2 core/shell nano-catalyst.

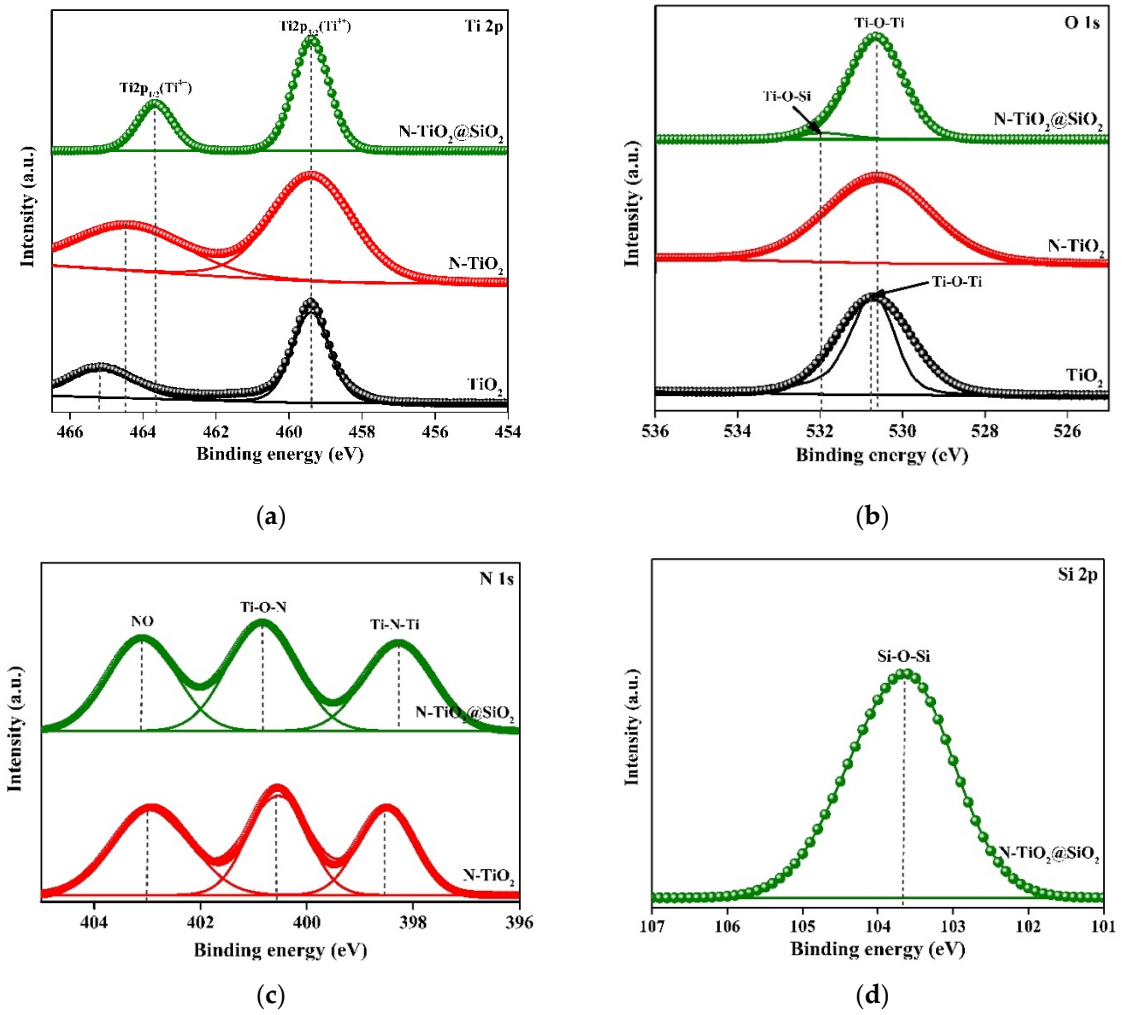

Figure 3. The XPS spectra of TiO_2, N-TiO_2, and N-TiO_2@SiO_2 core/shell for (**a**) Ti 2p, (**b**) O 1s, (**c**) N 1s, and (**d**) Si 2p.

2.1.4. Specific Surface Area and Porosity

N_2 adsorption-desorption isotherms and pore size distributions of TiO_2, N-TiO_2, and N-TiO_2@SiO_2 core/shell were measured by the BET method, as shown in Figure 4. All isotherms were classified as type IV in the IUPAC classification, referring to mesoporous material [43]. The isotherms of TiO_2 and N-TiO_2 had an H2a hysteresis loop, indicating the narrow pore diameter and complicated pore shape of mesoporous, whereas the core/shell N-TiO_2@SiO_2 isotherm displayed an H2b hysteresis loop, indicating a characteristic of mesoporous silica [44]. The pore size distributions of TiO_2, N-TiO_2, and N-TiO_2@SiO_2 core/shell were narrow, and the average pore diameters were in a range between 5–25 nm. According to BET analysis, the specific surface area of the N-TiO_2 nano-catalyst was increased from 40 m^2g^{-1} to 157 m^2g^{-1} after incorporating the SiO_2 shell. This result was in agreement with Mahanta et al., (2022) [34]. The large specific surface area could

promote the adsorbability and photocatalytic activity of the nano-catalyst, which would help improve the photocatalytic degradation of organic pollutants [45,46].

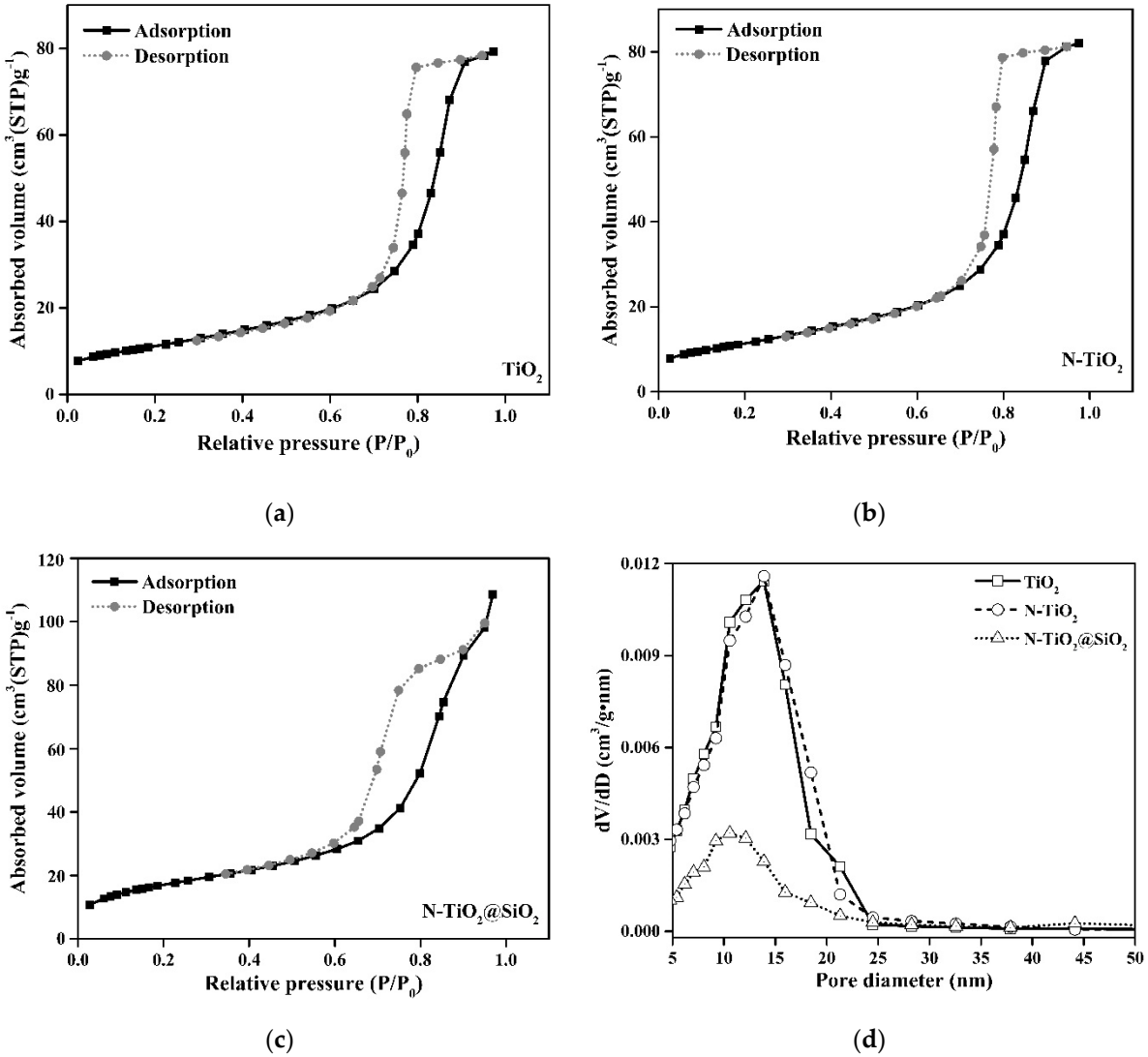

Figure 4. N_2 adsorption-desorption isotherms of (**a**) TiO_2, (**b**) N-TiO_2, (**c**) N-TiO_2@SiO_2 core/shell, and (**d**) pore size distribution.

2.1.5. Absorption Edge and Band Gap Energy

Figure 5 shows the UV-Vis-NIR spectra and Tauc plots (inset) of N-TiO_2 and N-TiO_2@SiO_2 core/shell, observed in the wavelength range of 200–700 nm. The absorption edge of the TiO_2@SiO_2 core/shell shifted to a lower wavelength than that of N-TiO_2, indicating the blue shift effect (increasing bandgap energy). The bandgap energy calculated by the Tauc plot of TiO_2@SiO_2 core/shell was 2.92 eV, while the bandgap energy of N-TiO_2 was 2.79 eV. The blue shift effect of the SiO_2 shell-coated N-TiO_2 core was caused by two mechanisms. Firstly, the addition of SiO_2 considerably reduced the particle size of the N-TiO_2@SiO_2, leading to the quantum size effect (from bulk to nanoparticles). Secondly, the change in the electronic structure of Ti-O-Si bonds found in the N-TiO_2@SiO_2 core/shell required higher energy for electrons moving from the valence band to the conduction band [47].

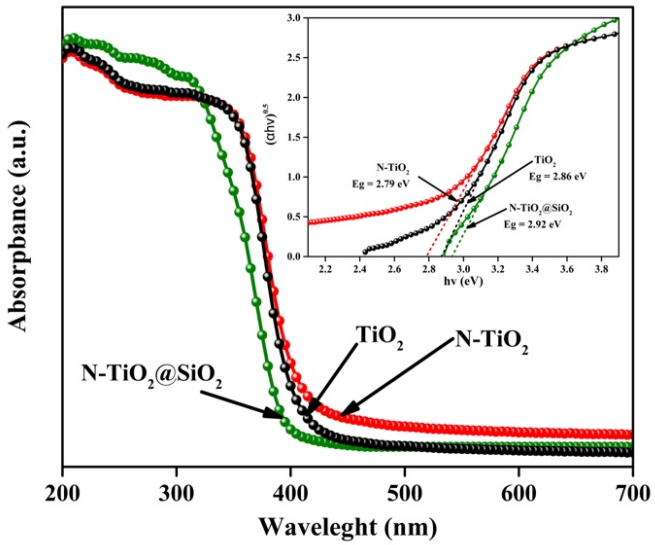

Figure 5. UV-Vis Near-Infrared spectrum and band gap energy calculated by Tauc plot (inset) of TiO_2, N-TiO_2, and core/shell N-TiO_2@SiO_2.

2.2. Photocatalytic Paint

2.2.1. Acid and Alkali Resistance

The results of acid and alkali resistance of the commercial paint (without photocatalyst), TiO_2, N-TiO_2, and N-TiO_2@SiO_2 photocatalytic paints are illustrated in Figures 6 and 7. After the samples were swamped in the acid and alkali solution for 18 h at room temperature, the swelling of the TiO_2 paint film and the crack of the N-TiO_2 paint film were observed, indicating no resistance to the acid and alkali solution. While no change on the film surface was observed on the samples coated by commercial and N-TiO_2@SiO_2 paints. Self-degradation in the paint can occur when the photocatalyst is exposed to light and water in the environment. The photocatalyst produces hydroxyl radicals and superoxides, which can degrade the organic compounds in the paint, resulting in self-degradation. The results infer that the TiO_2@SiO_2 core/shell structure provides an advantage in film protection. Without a SiO_2 shell, the photocatalyst could degrade organic binders. Furthermore, severe degradation was seen when the films were exposed to an acid and alkali solution, especially for the N-TiO_2 paint film.

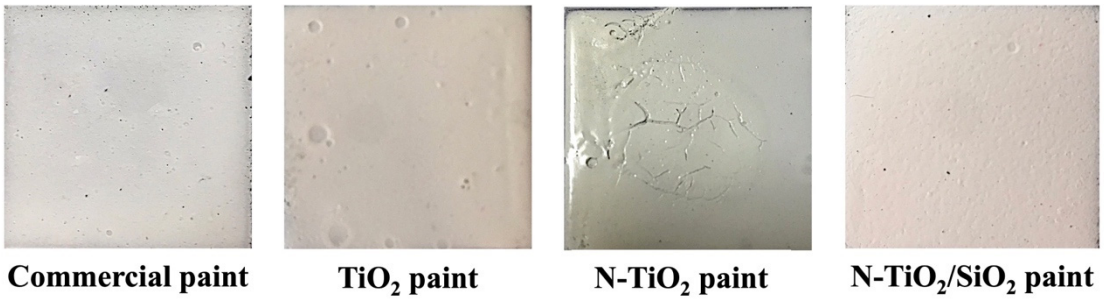

Figure 6. The acid resistance tests of commercial paint (without photocatalyst), TiO_2 paint, N-TiO_2 paint, and N-TiO_2@SiO_2 paint.

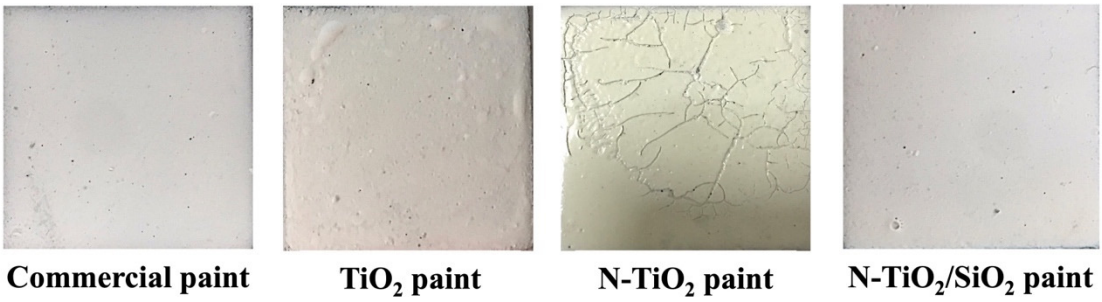

Figure 7. The alkali resistance tests of commercial paint (without photocatalyst), TiO_2 paint, N-TiO_2 paint, and N-TiO_2@SiO_2 paint.

2.2.2. Adhesion Test

The results of the cross-cut test are presented in Figure 8. The adhesion performance can be classified into six levels, including (5B) not removed, (4B) less than 5%, (3B) about 5–15%, (2B) 15–35%, (1B) 35–65%, and (0B) greater than 65%. The adhesion performances of all films were ranked from the highest to the lowest adhesion ability as follows: Commercial emulsion paint (5B), N-TiO_2@SiO_2 paint (4B), TiO_2 paint (3B), and N-TiO_2 paint (0B), respectively. The trend was similar to the results of acid and alkali resistance. The N-TiO_2 paint exhibited the worst performance because the photocatalytic reactivity of TiO_2 was enhanced by N doping. Due to the high photocatalytic reactivity of the N-TiO_2 photocatalyst, the organic binder tended to be easily degraded. Incorporating SiO_2 as a core in N-TiO_2 could significantly improve the chemical resistance and adhesion ability of the paint film. Similar to other studies, it was reported that the important role of the SiO_2 shell was preventing self-degradation in paint [35,48,49]. Since the acid and alkali resistance and adhesion performance of TiO_2@SiO_2 paint were comparable with commercial paint, the N-TiO_2@SiO_2 paint was proposed as a promising photocatalytic paint, especially for indoor applications.

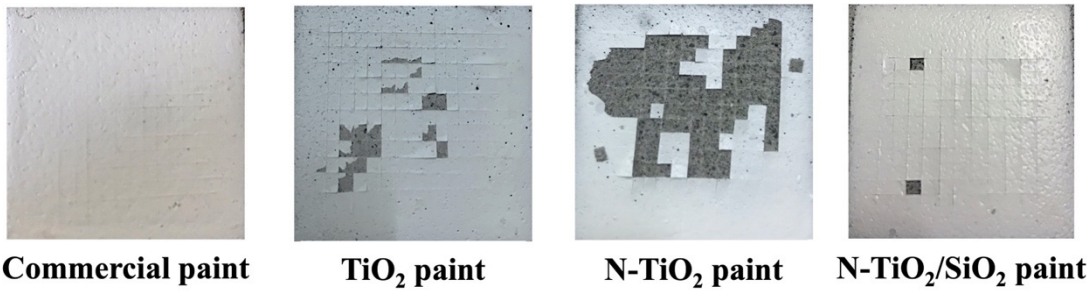

Figure 8. The adhesion tests of commercial paint (without photocatalyst), TiO_2 paint, N-TiO_2 paint, and N-TiO_2@SiO_2 paint.

2.2.3. Photocatalytic Decomposition of Gaseous Acetaldehyde

Figure 9 shows the acetaldehyde removal in the dark and under LED irradiation. In the dark, the adsorption capacity of N-TiO_2@SiO_2 paint (10.31%) was the highest, followed by N-TiO_2 paint (5.62%), TiO_2 paint (4.30%), and commercial paint (<1%), respectively. Similar to the adsorption in the dark, the N-TiO_2@SiO_2 paint exhibited the highest acetaldehyde degradation efficiency under LED irradiation (31.49%) compared with N-TiO_2 paint (17.71%) and TiO_2 paint (5.01%). It was clear that nitrogen doping on TiO_2 could significantly enhance the photocatalytic reactivity of TiO_2 under LED irradiation. When the nitrogen atom was doped into the TiO_2 structure, the new mid-band gap above the valence band of TiO_2 was created. This narrowed bandgap could facilitate the movement of electrons in the valence band to the conduction band under LED irradiation. Moreover, it was noted that incorporating a SiO_2 shell into TiO_2 could improve both the adsorption

capacity and photocatalytic reactivity of the photocatalyst. The impressive performance of N-TiO_2@SiO_2 paint was mainly contributed by the SiO_2 shell. The encapsulation of N-TiO_2 with a SiO_2 shell could increase the specific surface area of the catalyst and reduce particle aggregation. These advantages also help improve particle dispersion in the paint. Moreover, the SiO_2 shell could provide more reactive acid sites (silanol groups) and prevent charge recombination in photocatalysis.

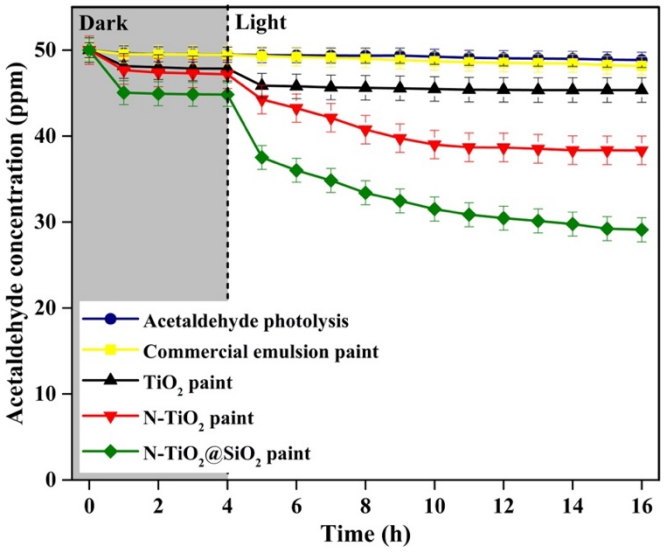

Figure 9. Adsorption (in the dark) and photocatalytic performance of gaseous acetaldehyde decomposition by different photocatalytic paints under LED visible light at room temperature within 16 h.

The comparison between the photocatalytic performance of N-TiO_2@SiO_2 paint in this study and other similar studies can be described as follows. Islam et al., (2020) [25] developed a photocatalytic paint based on TiO_2 and photopolymer resin. The photocatalytic performance of the paint was examined by photodegradation of MO and MB dye in water under UV-B and sunlight irradiation. This study found that the highest photodegradation efficiency of MO and MB dye in water under sunlight irradiation was approximately 90% in 60 min. Unlike the current study, the photocatalytic paint prepared by Islam et al., (2020) used a photopolymer resin as a binder, not a commercial emulsion paint. Moreover, the photocatalytic performance was tested under UV rather than visible light irradiation. This photocatalytic paint might be suitable for external uses. Basso et al., (2018) [26] used TiO_2 P25 powder as an additive in acrylic-based paint for toluene degradation. The photodegradation performance of toluene under UV-A irradiation was approximately 32.6% for 10 min. The results indicated the toluene degradation and the self-degradation of organic compounds in the paint composition; the N-TiO_2@SiO_2 photocatalytic paint prepared in this study could degrade acetaldehyde even under visible light irradiation without degrading an organic binder. Accordingly, the N-TiO_2@SiO_2 photocatalytic paint in this study is a promising material for commercial interior paint.

Apart from nitrogen dopant, Ag dopant is a promising metal used to improve the photocatalytic performance of TiO_2. Kumar et al., (2016) [50] studied Ag nanoparticle decorated TiO_2 nanorod array (Ag-TiO_2) substrates using a glancing angle deposition (GLAD) technique for photocatalysis and surface-enhanced Raman scattering (SERS) applications. The photocatalytic performance of the Ag-TiO_2 was evaluated by the degradation of rhodamine 6G (Rh6G) under UV irradiation. They reported that the Ag-TiO_2 could degrade 90% of Rh6G under UV irradiation within 90 min. Singh et al., (2018) [51] synthesised Ag-TiO_2 hybrid nanoparticles by CTAB-assisted wet chemical synthesis and applied the photocatalysts for the photocatalytic degradation of MB dye under solar light irradiation.

The results showed that the hybrid material could remove 89.2% of MB dye under solar light irradiation within 60 min, higher than bare TiO_2 (50.1%). Even though the Ag dopant could improve the photocatalytic reactivity of TiO_2, Ag played a different role when compared with N dopant. The N dopant helped uplift the valence band towards the conduction band [52], while the Ag dopant helped extend light absorption toward a visible region by surface plasmon resonance, as well as delay the recombination rate of electrons and holes of TiO_2 [29]. The pale yellow N-doped TiO_2 particles also had an advantage over the grey Ag-TiO_2 particles. The N-doped TiO_2 particles could be added without affecting the colour shade of the paint.

The kinetic reaction of photocatalytic degradation of acetaldehyde was studied using Equation (1)

$$\ln\left(\frac{C_0}{C}\right) = kt \quad (1)$$

where C_0 is the initial concentration of acetaldehyde (50 ppm), C is the concentration of acetaldehyde (ppm) after time (t), and k is the pseudo-first-order rate (h^{-1}). The photocatalytic degradation of acetaldehyde fits with a pseudo-first-order model, as shown in Figure 10. The calculated pseudo-first-order kinetic constants (k) of TiO_2 paint, N-TiO_2 paint, and N-TiO_2@SiO_2 paint were 0.0062 h^{-1}, 0.0228 h^{-1}, and 0.0455 h^{-1}, respectively. The reaction constant of N-TiO_2@SiO_2 paint was the highest and nearly two times higher than that of N-TiO_2 paint.

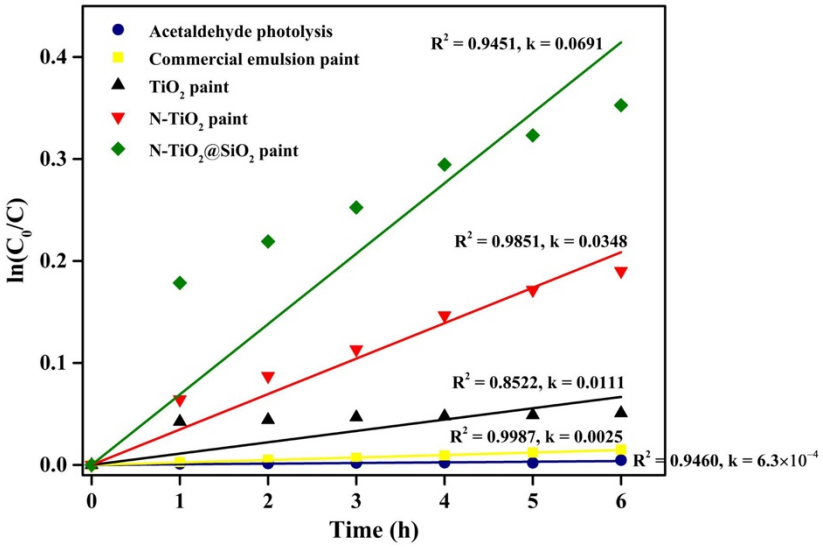

Figure 10. Pseudo-first-order models of gaseous acetaldehyde photodegradation by different photocatalytic paints under LED visible light at room temperature within 6 h.

Figure 11 illustrates the hypothesised mechanism of acetaldehyde photocatalytic degradation using N-TiO_2@SiO_2 paint. The N doping on the TiO_2 structure creates a new mid-band gap above the valence band (VB) of TiO_2. The LED light energises electrons in the VB, and then the excited electrons move to the conduction band (CB), leaving the hole (h^+) in the VB. The SiO_2 shell coated on the N-TiO_2 core helps increase the adsorption of the acetaldehyde molecules on the film surface. The excited electrons in the VB react with oxygen (O_2) in the air, generating superoxide radicals (O_2^-), while the H_2O molecules adsorbed by h^+ in the CB produce hydroxyl radicals ($OH^\bullet$). Both active radicals decompose the gaseous acetaldehyde molecules into various small molecules and, finally, into CO_2 and H_2O. The hypothesised decomposition mechanism is described in Equation (2) [53].

$$\begin{aligned} CH_3CHO + OH^\bullet &\rightarrow CH_3COOH \\ CH_3COOH + OH^\bullet &\rightarrow CH_2O \\ CH_2O + OH^\bullet &\rightarrow CH_2O_2 \\ CH_2O_2 + OH^\bullet &\rightarrow CO_2 + H_2O \end{aligned} \quad (2)$$

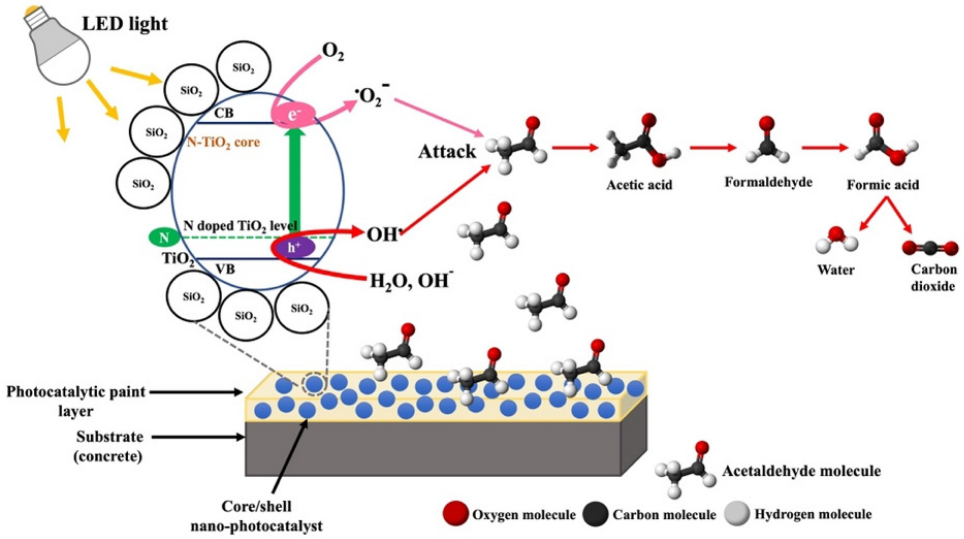

Figure 11. Schematic illustration of a photocatalytic mechanism for decomposition of gaseous acetaldehyde by N-TiO_2@SiO_2 paint.

3. Materials and Methods

3.1. Materials

Titanium (IV) butoxide (TBOT, 97%) was purchased from Sigma-Aldrich (St. Louis, MO, USA). Ethanol (99.8%), Nitric acid (HNO_3), and Hydrochloric acid (HCl, 37%) were purchased from Qrec (New Zealand). Diethylene-amine (DEA, 99%), Tetraethyl orthosilicate (TEOS, 99.99%), Methylene blue (MB) ($C_6H_{18}N_3ClS.2H_2O$, ≥96%), and Acetaldehyde (CH_3CHO, ≥99.5%) were purchased from Merck (Rahway, NJ, USA). These chemicals were used for the synthesis of the core/shell nano-photocatalyst.

Ammonia (NH_3, 25%) was purchased from Qrec, New Zealand. Polycarboxylic acid sodium salt (CARRYBON L-400) used as a dispersing agent was purchased from Sanyo Kasei Ltd. (Bankhai, RYG, Thailand), ULTRABOND P261 acrylic, Hydroxyethyl cellulose (cellosize), and water treatment defoamer (E-193) were purchased from Chemical Village Co., Ltd. (Bangplee, SPK, Thailand). These chemicals were used to prepare the photocatalytic paint. Finally, calcium hydroxide ($Ca(OH)_2$) was purchased from Merck (Rahway, NJ, USA) and used for the alkali resistance test.

3.2. Nano-Photocatalyst Preparations

TiO_2 and N-doped TiO_2 photocatalysts were synthesised by the solvothermal method, and then N-doped TiO_2@SiO_2 core/shell photocatalysts were synthesised by the sol-gel method, following [33,54]. The molar ratios of the synthesised photocatalysts were $1Ti(OC_4H_9)_4$:$18C_2H_5OH$:$2H_2O$:$0.2HNO_3$. TBOT was dissolved in ethanol and then the nitric solution was added to the TBOT solution. The solution was stirred at room temperature for 2 h and then transferred into a Teflon-lined stainless-steel autoclave. The autoclave was placed in an oven and heated to 150 °C for 5 h. After that, the suspended solid was separated by a centrifuge and washed with DI water and ethanol before being calcined at 450 °C for 3 h. The obtained white powder was TiO_2 photocatalyst. To prepare an N-doped TiO_2 (named N-TiO_2) photocatalyst, 5% mol of DEA in ethanol was added to the TBOT solution before being transferred to an autoclave.

The synthesis of the N-doped TiO_2@SiO_2 core/shell nano-photocatalyst (N-TiO_2@SiO_2) was modified from [33,54]. TEOS, as a SiO_2 precursor, was dissolved in 50 mL of ethanol solution, and then the N-TiO_2 photocatalyst was added into the TEOS solution (molar ratio of Ti:Si = 1:1.5). The pH of the mixture was then adjusted to 10 by adding 1 M of HCl. The solution was constantly stirred at 80 °C for 17 h to complete the synthesis reaction. The suspended solid was then precipitated using a centrifuge, washed with DI water, and calcined at 550 °C for 2 h. The final product was the N-TiO_2@SiO_2 core/shell nano-photocatalyst.

3.3. Nano-Photocatalyst Characterizations

The crystal structures of all nano-photocatalysts were investigated by an X-ray diffractometer (XRD, D8 Advance with Eulerian Cradle, Bruker, Billerica, MA, USA) with Cu Kα radiation (λ = 1.54 Å). The morphology was observed via Field Transmission Electron Microscopy (FE-TEM, JEM-3100F, Tokyo, Japan). The specific surface area was determined from the Brunauer-Emmett-Teller (BET) method by N_2 gas adsorption-desorption isotherms at 77 K with a surface analyser (Autosorb-1, Quantachrome, BEL model, Waltham, MA, USA). The pore size distribution was evaluated from the N_2 desorption by the Barrett-Joyner-Halenda (BJH) method. The elemental composition was obtained using energy dispersive X-ray spectroscopy (EDX, Oxford, INCAx-act, Tokyo, Japan) and X-ray photoelectron spectroscopy (XPS). The absorption edge was analysed by an Ultraviolet-Visible-Near Infrared (UV-VIS-NIR, Perkin Elmer, Lambda 950, Waltham, MA, USA) spectrometer within the range of 300–800 nm.

3.4. Photocatalytic Paint Preparation

Photocatalytic paint, with and without photocatalysts, was prepared using the following commercial formula, as shown in Table 1. Bare TiO_2, N-TiO_2, and N-TiO_2@SiO_2 core/shell nano-photocatalysts were used as paint additives. The procedure for the photocatalytic paint preparation is illustrated in Figure 12. The nano-photocatalyst powder was dispersed in DL water by homogeniser at 4000 rpm for 30 min. CARRYBON L-400, E-193, and cellosize were added to the nano-photocatalyst solution. After that, the slurry mixture was stirred by a homogeniser at 4000 rpm for 45 min. Then, NH_3, E-193, and acrylic P261 were added to the slurry mixture and stirred by a homogeniser at 6000 rpm for 1 h. The final products were photocatalytic paints.

Table 1. Formulation of the photocatalytic paint.

Ingredient of Photocatalytic Paint	wt.%
Nano-photocatalyst powder	3.60
DI water	72.53
Dispersing agent (CARRYBON L-400)	0.36
Defoamer (E-193)	0.54
Cellosize	1.08
NH_3	0.18
Acrylic (P261)	21.71
Total	100

3.5. Standard Testing of the Photocatalytic Paints

The acid and base resistance of the prepared photocatalytic paint was tested following the Thai Industrial Standards (TIS) no. 2321, while the adhesion performance of the paint film was evaluated following International Standards no. ASTM D 3359-22 (Standard Test Methods for Rating Adhesion by Tape Test). Square concrete samples 3 cm × 3 cm in size were coated with the photocatalytic paints (TiO_2, N-TiO_2, and N-TiO_2@SiO_2) and commercial emulsion paint (without photocatalyst), and then dried at room temperature for 2 days. For the acid resistance test, the samples were soaked with a 5% w/v HCl solution for 18 h (pH 3–5). For the alkali resistance test, the samples were soaked with a $Ca(OH)_2$ solution (pH 10–12) for 18 h. The adhesion test was performed by the cross-cut tape method. The surface of the coated samples was scratched into 11 horizontal and 11 vertical grid lines using a cutter. Then, clear adhesive tape was placed on the cross-cut area and pulled in 1 s. The adhesion test results could be observed from the percentages of the removed film, which were classified into six levels, including (5B) not removed, (4B) less than 5%, (3B) about 5–15%, (2B) 15–35%, (1B) 35–65%, and (0B) greater than 65%, respectively. All tests were performed in triplicate.

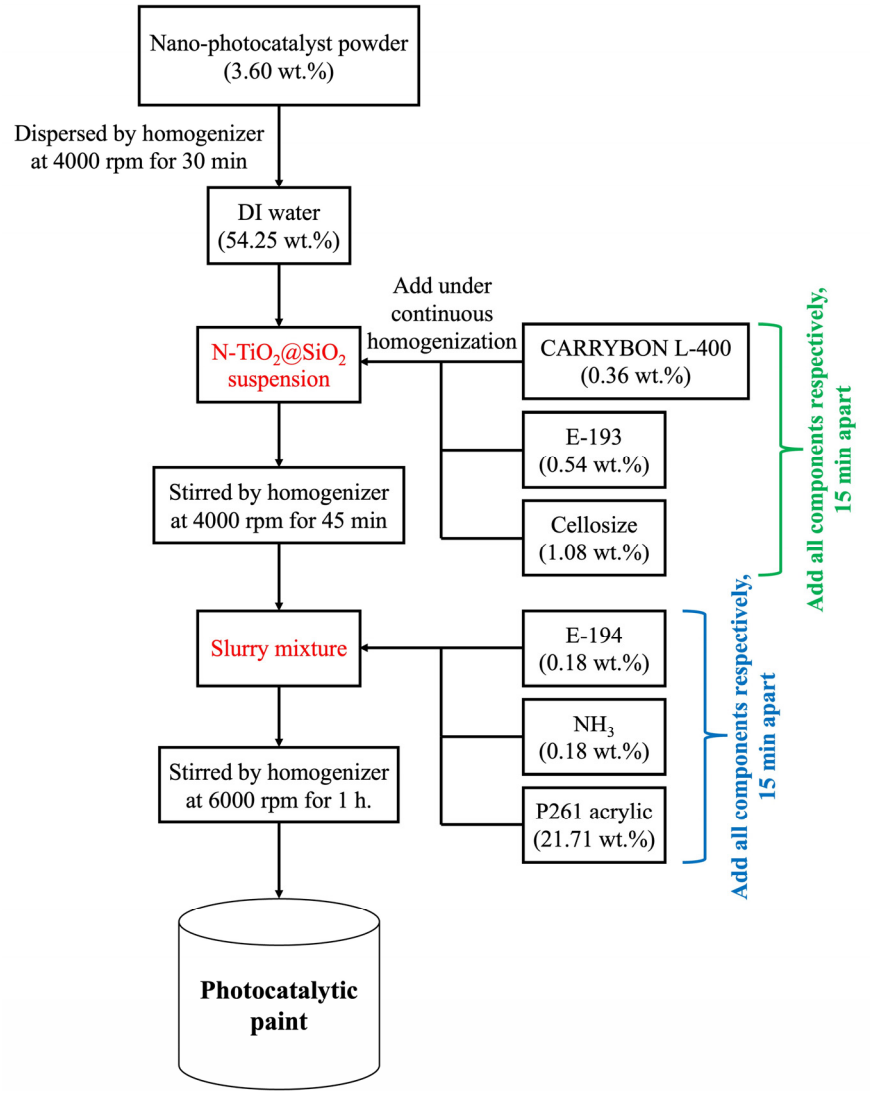

Figure 12. Schematic illustration of nano-catalyst paint preparation.

3.6. Photocatalytic Decomposition of Gaseous Acetaldehyde

The photocatalytic decomposition of gaseous acetaldehyde by the photocatalytic paint was carried out in a closed stainless-steel reactor (volume 54 L) equipped with two 16 W LED visible lamps (wavelength 365–800 nm) and two 220 V blower fans for simulating air circulation (see Figure 13). Two pieces of 24 cm × 24 cm glass plates and two pieces of 24 cm × 54 cm with a total area of 1872 cm^2 were coated with 300 mL of the photocatalytic paint and placed beside the walls in a closed stainless-steel reactor. The reactor was loaded with gaseous acetaldehyde (50 ppm) in the dark. To determine the adsorption capacity, gas samples were collected every hour to evaluate the acetaldehyde concentration by gas chromatography with a flame ionisation detector (GC-FID, model GC-14B, Shimadzu, Kyoto, Japan). When the adsorption was completed, two LED lamps were turned on and acetaldehyde gas was collected and analysed using GC-FID every hour to determine the photodegradation efficiency.

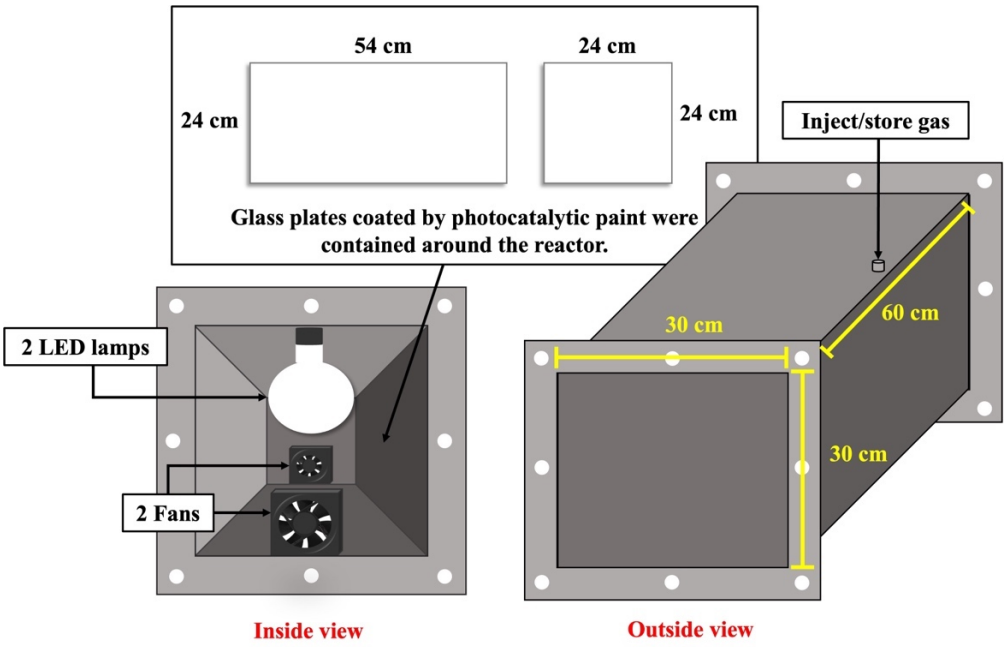

Figure 13. Schematic illustration of a closed stainless-steel reactor (inside and outside views).

4. Conclusions

In this study, the N-TiO_2@SiO_2 core/shell nano-photocatalyst was synthesised via the solvothermal method and applied as an additive to produce photocatalytic paint. The photocatalytic paint was applied for gaseous acetaldehyde decomposition under LED irradiation. The results indicated the advantage of N-TiO_2 over TiO_2. Nitrogen atoms inside the TiO_2 lattice played an important role in creating a new mid-band gap above the valence band (VB) of TiO_2, which brought about the reduction of bandgap energy. Moreover, encapsulating the N-TiO_2 core with a SiO_2 shell exhibited superior photocatalytic performance when compared to bare N-TiO_2. The SiO_2 shell helped to increase the specific surface area, as well as reduce aggregation and prevent charge recombination in photocatalytic reactions. Additionally, the SiO_2 shell could reduce the self-degradation problem in the photocatalytic paint. The acid and alkali resistance, as well as the adhesion ability, of the N-TiO_2@SiO_2 paint were excellent and comparable with commercial paint (without a photocatalyst). Thus, N-TiO_2@SiO_2 visible-light responsive paint is recommended as a promising photocatalytic paint used for indoor air purification.

Supplementary Materials: The following are available online at https://www.mdpi.com/article/10.3390/catal13020351/s1, Figure S1: The particle size distributions of (a) TiO_2, (b) N-TiO_2, and (c) N-TiO_2@SiO_2; Figure S2: SEM images of (a) TiO_2, (b) N-TiO_2, and (c) N-TiO2@SiO2; Figure S3: The EDX spectrum of (a) N-TiO_2 and (b) N-TiO_2@SiO_2 core/shell.

Author Contributions: S.C. was in charge of a research supervisor and acted as a corresponding author. T.A. was responsible for the data validation. S.S. was responsible for conducting the experiments and preparing the manuscript. All authors have read and agreed to the published version of the manuscript.

Funding: This research was supported by the Joint Graduate School of Energy and Environment, King Mongkut's University of Technology Thonburi, Centre of Excellence on Energy Technology and Environment, PERDO, Thailand, the Research and Researcher for Industries (RRI) scholarship from Thailand Research Fund (TRF) under grant number PHD61I0007, and Thailand Science Research and Innovation (TSRI) Basic Research Fund: The fiscal year 2022 under project number FRB650048/0164.

Data Availability Statement: The datasets generated during the current study are available from the corresponding author upon reasonable request.

Conflicts of Interest: All authors declare no conflict of interest.

References

1. Austin, B.S.; Greenfield, S.M.; Weir, B.R.; Anderson, G.E.; Behar, J.V. Modeling the indoor environment. *Environ. Sci. Technol.* **1992**, *26*, 850–858. [CrossRef]
2. Yu, B.F.; Hu, Z.B.; Liu, M.; Yang, H.L.; Kong, Q.X.; Liu, Y.H. Review of research on air-conditioning systems and indoor air quality control for human health. *Int. J. Refrig.* **2009**, *32*, 3–20. [CrossRef]
3. Zhong, L.; Haghighat, F. Photocatalytic air cleaners and materials technologies–abilities and limitations. *Build. Environ.* **2015**, *91*, 191–203. [CrossRef]
4. Saini, J.; Dutta, M.; Marques, G. A comprehensive review on indoor air quality monitoring systems for enhanced public health. *Sustain. Environ. Res.* **2020**, *30*, 1–12. [CrossRef]
5. Marć, M.; Śmiełowska, M.; Namieśnik, J.; Zabiegała, B. Indoor air quality of everyday use spaces dedicated to specific purposes–a review. *Environ. Sci. Pollut. Res.* **2018**, *25*, 2065–2082. [CrossRef]
6. Peng, Z.; Deng, W.; Tenorio, R. Investigation of indoor air quality and the identification of influential factors at primary schools in the North of China. *Sustainability* **2017**, *9*, 1180. [CrossRef]
7. Liu, S.; Li, R.; Wild, R.J.; Warneke, C.; De Gouw, J.A.; Brown, S.S.; Miller, S.L.; Luongo, J.C.; Jimenez, J.L.; Ziemann, P.J. Contribution of human-related sources to indoor volatile organic compounds in a university classroom. *Indoor Air* **2016**, *26*, 925–938. [CrossRef]
8. Dunagan, S.C.; Dodson, R.E.; Rudel, R.A.; Brody, J.G. Toxics use reduction in the home: Lessons learned from household exposure studies. *J. Clean. Prod.* **2011**, *19*, 438–444. [CrossRef]
9. Burge, P.S. Sick building syndrome. *Occup. Environ. Med.* **2004**, *61*, 185–190. [CrossRef]
10. Kim, J.M.; Kim, J.H.; Lee, C.Y.; Jerng, D.W.; Ahn, H.S. Toluene and acetaldehyde removal from air on to graphene-based adsorbents with microsized pores. *J. Hazard. Mater.* **2018**, *344*, 458–465. [CrossRef]
11. Paschke, T.; Scherer, G.; Heller, W.D. Effects of ingredients on cigarette smoke composition and biological activity: A literature overview. *Beitr. Tabakforsch. Int./Contrib. Tob. Res.* **2002**, *20*, 107–247. [CrossRef]
12. Seeman, J.I.; Dixon, M.; Haussmann, H.J. Acetaldehyde in mainstream tobacco smoke: Formation and occurrence in smoke and bioavailability in the smoker. *Chem. Res. Toxicol.* **2002**, *15*, 1331–1350. [CrossRef] [PubMed]
13. Pennings, J.L.; Cremers, J.W.; Becker, M.J.; Klerx, W.N.; Talhout, R. Aldehyde and volatile organic compound yields in commercial cigarette mainstream smoke are mutually related and depend on the sugar and humectant content in tobacco. *Nicotine Tob. Res.* **2020**, *22*, 1748–1756. [CrossRef] [PubMed]
14. Galanti, L.M. Tobacco smoking cessation management: Integrating varenicline in current practice. *Vasc. Health Risk Manage.* **2008**, *4*, 837. [CrossRef] [PubMed]
15. Liu, G.; Xiao, M.; Zhang, X.; Gal, C.; Chen, X.; Liu, L.; Pan, S.; Wu, J.; Tang, L.; Clements-Croome, D. A review of air filtration technologies for sustainable and healthy building ventilation. *Sustain. Cities Soc.* **2017**, *32*, 375–396. [CrossRef]
16. Xiang, W.; Zhang, X.; Chen, K.; Fang, J.; He, F.; Hu, X.; Tsang, D.C.; Ok, Y.S.; Gao, B. Enhanced adsorption performance and governing mechanisms of ball-milled biochar for the removal of volatile organic compounds (VOCs). *Chem. Eng. J.* **2020**, *385*, 123842. [CrossRef]
17. Zhong, L.; Haghighat, F. Ozonation air purification technology in HVAC applications. *Ashrae Trans.* **2014**, *120*, 1–6.
18. Lin, L.; Chai, Y.; Zhao, B.; Wei, W.; He, D.; He, B.; Tang, Q. Photocatalytic oxidation for degradation of VOCs. *Open J. Inorg. Chem.* **2013**, *3*, 14–25. [CrossRef]
19. Pelaez, M.; Nolan, N.T.; Pillai, S.C.; Seery, M.K.; Falaras, P.; Kontos, A.G.; Dunlop, P.S.; Hamilton, J.W.; Byrne, J.A.; O'shea, K.; et al. A review on the visible light active titanium dioxide photocatalysts for environmental applications. *Appl. Catal. B.* **2012**, *125*, 331–349. [CrossRef]
20. Hashimoto, K.; Irie, H.; Fujishima, A. TiO_2 photocatalysis: A historical overview and future prospects. *Jpn. J. Appl. Phys.* **2005**, *44*, 8269. [CrossRef]
21. Zeng, Q.; Wang, X.; Xie, X.; Mahmood, A.; Lu, G.; Wang, Y.; Sun, J. Band bending of TiO_2 induced by O-xylene and acetaldehyde adsorption and its effect on the generation of active radicals. *J. Colloid. Interface. Sci.* **2020**, *572*, 374–383. [CrossRef] [PubMed]
22. Katsumata, K.I.; Hou, X.; Sakai, M.; Nakajima, A.; Fujishima, A.; Matsushita, N.; MacKenzie, K.J.D.; Okada, K. Visible-light-driven photodegradation of acetaldehyde gas catalyzed by aluminosilicate nanotubes and Cu(II)-grafted TiO_2 composites. *Appl. Catal. B* **2013**, *138–139*, 243–252. [CrossRef]
23. Sumran, M.; Kongkachuichy, P. Synthesis of silica from rice husks by one step combustion fluidized bed combustion and alkaline extraction. *In KKU Eng. J.* **2003**, *30*, 165–172.
24. Park, H.; Park, Y.; Kim, W.; Choi, W. Surface modification of TiO_2 photocatalyst for environmental applications. *J. Photochem. Photobiol. C.* **2013**, *15*, 1–20. [CrossRef]
25. Islam, M.T.; Dominguez, A.; Turley, R.S.; Kim, H.; Sultana, K.A.; Shuvo, M.A.I.; Alvarado-Tenorio, B.; Montes, M.O.; Lin, Y.; Gardea-Torresdey, J.; et al. Development of photocatalytic paint based on TiO_2 and photopolymer resin for the degradation of organic pollutants in water. *Sci. Total Environ.* **2020**, *704*, 135406. [CrossRef]
26. Basso, A.; Battisti, A.P.; Moreira, R.; de, F.P.M.; José, H.J. Photocatalytic effect of addition of TiO_2 to acrylic-based paint for passive toluene degradation*. *Environ. Technol.* **2020**, *41*, 1568–1579. [CrossRef]

27. Meroni, D.; Ardizzone, S.; Cappelletti, G.; Oliva, C.; Ceotto, M.; Poelman, D.; Poelman, H. Photocatalytic removal of ethanol and acetaldehyde by N-promoted TiO_2 films: The role of the different nitrogen sources. *Catal. Today* **2011**, *161*, 169–174. [CrossRef]
28. He, F.; Ma, F.; Li, T.; Li, G. Solvothermal synthesis of N-doped TiO_2 nanoparticles using different nitrogen sources, and their photocatalytic activity for degradation of benzene. *Chin. J. Catal.* **2013**, *34*, 2263–2270. [CrossRef]
29. Sirivallop, A.; Areerob, T.; Chiarakorn, S. Enhanced visible light photocatalytic activity of N and Ag doped and co-doped TiO_2 synthesized by using an in-situ solvothermal method for gas phase ammonia removal. *Catalysts* **2020**, *10*, 251. [CrossRef]
30. Guo, N.; Liang, Y.; Lan, S.; Liu, L.; Ji, G.; Gan, S.; Zou, H.; Xu, X. Uniform TiO_2-SiO_2 hollow nanospheres: Synthesis, characterization and enhanced adsorption-photodegradation of azo dyes and phenol. *Appl. Surf. Sci.* **2014**, *305*, 562–574. [CrossRef]
31. Nadrah, P.; Gaberšček, M.; Sever Škapin, A. Selective degradation of model pollutants in the presence of core@shell TiO_2@SiO_2 photocatalyst. *Appl. Surf. Sci.* **2017**, *405*, 389–394. [CrossRef]
32. Jiang, Q.; Huang, J.; Ma, B.; Yang, Z.; Zhang, T.; Wang, X. Recyclable, hierarchical hollow photocatalyst TiO_2@SiO_2 composite microsphere realized by raspberry-like SiO_2. *Colloids. Surf. A* **2020**, *602*, 125112. [CrossRef]
33. Gholami, T.; Bazarganipour, M.; Salavati-Niasari, M.; Bagheri, S. Photocatalytic degradation of methylene blue on TiO_2@SiO_2 core/shell nanoparticles: Synthesis and characterization. *J. Mater. Sci. Mater. Electron.* **2015**, *26*, 6170–6177. [CrossRef]
34. Mahanta, U.; Khandelwal, M.; Deshpande, A.S. TiO_2@SiO_2 nanoparticles for methylene blue removal and photocatalytic degradation under natural sunlight and low-power UV light. *Appl. Surf. Sci.* **2022**, *576*, 151745. [CrossRef]
35. Wang, D.; Geng, Z.; Hou, P.; Yang, P.; Cheng, X.; Huang, S. Rhodamine B removal of TiO_2@SiO_2 core-shell nanocomposites coated to buildings. *Crystals* **2020**, *10*, 80. [CrossRef]
36. Koli, V.B.; Mavengere, S.; Kim, J.S. An efficient one-pot N doped TiO_2-SiO_2 synthesis and its application for photocatalytic concrete. *Appl. Surf. Sci.* **2019**, *491*, 60–66. [CrossRef]
37. Sun, J.; Xu, K.; Shi, C.; Ma, J.; Li, W.; Shen, X. Influence of core/shell TiO_2@SiO_2 nanoparticles on cement hydration. *Constr. Build. Mater.* **2017**, *156*, 114–122. [CrossRef]
38. Zhang, H.; Luo, X.; Xu, J.; Xiang, B.; Yu, D. Synthesis of TiO_2/SiO_2 Core/Shell Nanocable Arrays. *J. Phys. Chem. B* **2004**, *108*, 14866–14869. [CrossRef]
39. Yang, J.; Bai, H.; Jiang, Q.; Lian, J. Visible-light photocatalysis in nitrogen–carbon-doped TiO_2 films obtained by heating TiO_2 gel–film in an ionized N_2 gas. *Thin Solid Films* **2008**, *516*, 1736–1742. [CrossRef]
40. Wang, X.; Lim, T.T. Solvothermal synthesis of C–N codoped TiO_2 and photocatalytic evaluation for bisphenol A degradation using a visible-light irradiated LED photoreactor. *Appl. Catal. B* **2010**, *100*, 355–364. [CrossRef]
41. Popa, M.; Macovei, D.; Indrea, E.; Mercioniu, I.; Popescu, I.C.; Danciu, V. Synthesis and structural characteristics of nitrogen doped TiO_2 aerogels. *Microporous Mesoporous Mater* **2010**, *132*, 80–86. [CrossRef]
42. Chen, Y.; Tang, X.; Gao, X.; Zhang, B.; Luo, Y.; Yao, X. Antimicrobial property and photocatalytic antibacterial mechanism of the TiO_2-doped SiO_2 hybrid materials under ultraviolet-light irradiation and visible-light irradiation. *Ceram. Int.* **2019**, *45*, 15505–15513. [CrossRef]
43. Fatimah, I.; Prakoso, N.I.; Sahroni, I.; Musawwa, M.M.; Sim, Y.L.; Kooli, F.; Muraza, O. Physicochemical characteristics and photocatalytic performance of TiO_2/SiO_2 catalyst synthesized using biogenic silica from bamboo leaves. *Heliyon* **2019**, *5*, e02766. [CrossRef]
44. Thommes, M.; Kaneko, K.; Neimark, A.V.; Olivier, J.P.; Rodriguez-Reinoso, F.; Rouquerol, J.; Sing, K.S. Physisorption of gases, with special reference to the evaluation of surface area and pore size distribution (IUPAC Technical Report). *Pure Appl. Chem.* **2015**, *87*, 1051–1069. [CrossRef]
45. Fu, X.; Clark, L.A.; Yang, Q.; Anderson, M.A. Enhanced Photocatalytic Performance of Titania-Based. *Environ. Sci. Technol.* **1996**, *30*, 647–653. [CrossRef]
46. Kumar, S.; Terashima, C.; Fujishima, A.; Krishnan, V.; Pitchaimuthu, S. Photocatalytic degradation of organic pollutants in water using graphene oxide composite. In *A new Generation Material Graphene: Applications in Water Technology*; Springer: Cham, Switzerland, 2019; pp. 413–438.
47. Van Grieken, R.; Aguado, J.; López-Muoz, M.J.; Marugán, J. Synthesis of size-controlled silica-supported TiO_2 photocatalysts. *J. Photochem. Photobiol. A.* **2002**, *148*, 315–322. [CrossRef]
48. Wei, X.; Xu, X.; Wu, J.; Li, C.; Chen, J.; Lv, B.; Zhu, B.; Xiang, H. SiO_2-modified nanocomposite nanofiltration membranes with high flux and acid resistance. *J. Appl. Polym. Sci.* **2019**, *136*, 47436. [CrossRef]
49. Amorim, S.M.; Suave, J.; Andrade, L.; Mendes, A.M.; Jose, H.J.; Moreira, R.F. Towards an efficient and durable self-cleaning acrylic paint containing mesoporous TiO_2 microspheres. *Prog. Org. Coat.* **2018**, *118*, 48–56. [CrossRef]
50. Kumar, S.; Lodhi, D.K.; Singh, J.P. Highly sensitive multifunctional recyclable Ag–TiO_2 nanorod SERS substrates for photocatalytic degradation and detection of dye molecules. *RSC Adv.* **2016**, *6*, 45120–45126. [CrossRef]
51. Singh, J.; Tripathi, N.; Mohapatra, S. Synthesis of Ag–TiO2 hybrid nanoparticles with enhanced photocatalytic activity by a facile wet chemical method. *Nano-Struct. Nano-Objects* **2019**, *18*, 100266. [CrossRef]
52. Samsudin, E.M.; Abd Hamid, S.B. Effect of band gap engineering in anionic-doped TiO2 photocatalyst. *Appl. Surf. Sci.* **2017**, *391*, 326–336. [CrossRef]

53. Zeng, Q.; Xie, X.; Wang, X.; Wang, Y.; Lu, G.; Pui, D.Y.H.; Sun, J. Enhanced photocatalytic performance of Ag@TiO_2 for the gaseous acetaldehyde photodegradation under fluorescent lamp. *Chem. Eng. J.* **2018**, *341*, 83–92. [CrossRef]
54. Padovini, D.S.S.; Magdalena, A.G.; Capeli, R.G.; Longo, E.; Dalmaschio, C.J.; Chiquito, A.J.; Pontes, F.M. Synthesis and characterization of ZrO_2@SiO_2 core-shell nanostructure as nanocatalyst: Application for environmental remediation of rhodamine B dye aqueous solution. *Mater. Chem. Phys.* **2019**, *233*, 1–8. [CrossRef]